IAHR AIRH

Journal of Hydraulic Research Vol. 47, No. 4 (2009), pp. 445–454
doi:10.3826/jhr.2009.3429

Impact of stem flexibility on mean flow and turbulence structure in depth-limited open channel flows with submerged vegetation

Impact de la flexibilité de tige sur l'écoulement moyen et la structure de la turbulence dans un canal de profondeur limitée avec de la végétation submergée

WONJUN YANG, IAHR Member, Post Doctoral Research Fellow, *School of Civil and Environmental Engineering, Yonsei University, Seoul 120-749, Korea. Tel.: +82 2 2123 2797; fax: +82 2 364 5300; e-mail: pulip@yonsei.ac.kr*

SUNG-UK CHOI, IAHR Member, Professor, *School of Civil and Environmental Engineering, Yonsei University, Seoul 120-749, Korea. E-mail: schoi@yonsei.ac.kr*

ABSTRACT
This study presents the results of laboratory experiments on depth-limited open channel flow with submerged vegetation. To investigate the impact of stem flexibility on the mean flow and turbulence structures, two flow types with similar drags but with flexible and rigid stems are compared. It is found that the stem flexibility hardly affects the mean flow but increases the peak value of the Reynolds shear stress. In addition, the stem flexibility increases and decreases the streamwise component of the turbulent intensity in the upper and vegetation layers, respectively. However, the stem flexibility increases the vertical component of the turbulent intensity over the whole depth. General profiles of the mean flow, the Reynolds shear stress, and the turbulent intensity are presented. The results of a quadrant analysis and a budget analysis are also provided.

RÉSUMÉ
Cette étude présente les résultats d'expériences de laboratoire sur l'écoulement en canal de profondeur limitée avec de la végétation submergée. Pour étudier l'impact de la flexibilité de tige sur les structures moyennes d'écoulement et de turbulence, on compare deux types d'écoulement avec des trainées semblables mais des tiges flexibles et rigides. On constate que la flexibilité de tige affecte à peine l'écoulement moyen mais augmente la valeur maximale de l'effort de cisaillement de Reynolds. En outre, la flexibilité de tige augmente l'intensité turbulente dans le sens de l'écoulement au niveau de la couche supérieure et la diminue dans la couche de la végétation. Par contre, la flexibilité de tige augmente la composante verticale de l'intensité turbulente dans la profondeur entière. Des profils généraux de l'écoulement moyen, de l'effort de cisaillement de Reynolds, et de l'intensité turbulente sont présentés. Les résultats d'une analyse de quadrant et d'une analyse de budget sont également fournis.

Keywords: Open channel flow, Stem flexibility, Submerged vegetation, Turbulence, Vegetated flow

1 Introduction

Vegetation in a watercourse increases flow resistance. Stems of vegetation generate wake turbulence, and the associated energy loss retards the mean flow. If vegetation is submerged, the enhanced turbulence shear production due to drag discontinuity plays the same role. This affects the conveyance of the channel.

Vegetated open channel flows are categorized into three types, namely terrestrial canopy flow, depth-limited flow with submerged vegetation, and flow through emergent vegetation (Nepf and Vivoni 2000). Terrestrial canopy flows result when the depth ratio H/h_1 is very large, where, H and h_1 denote the total flow depth and the height of the vegetation layer, respectively. Flows of this type are similar to open channel flows over rough beds. If the depth ratio is close to unity, the flow is discharged through emergent vegetation, in which shear production is absent. Such flows are characterized by reduced mean flow and turbulent intensities. Of particular interest are depth-limited open channel flows with submerged vegetation. The structure of such flows differs greatly from that of plain open channel flows. Flows within and above vegetation are markedly different; they have been described with the mixing layer analogy by Finnigan (2000) and the two-layer approach of Huthoff *et al*. (2007). Figure 1 shows a schematic sketch of a depth-limited open channel flow with submerged vegetation. For rigid stems, the height of the vegetation layer h_1 is equal to the vegetation height h_p. However, for flexible stems, h_1 is less than or equal to h_p. The flow structure within and above the vegetation layer largely depends on the drag due to vegetation.

Previous studies addressed the mean flow and turbulence structures of vegetated flows. Either rigid cylinders (Tsujimoto *et al*. 1992, Lopez and Garcia 1998, Okabe *et al*. 2000, Carollo *et al*. 2002, Nezu and Onitsuka 2001, Stone and Shen 2002, Choi *et al*. 2003, James *et al*. 2003, Ghisalberti and Nepf, 2004) or flexible plant mimics (Ikeda and Kanazawa 1996, Nepf and Vivoni 2000, Ghisalberti and Nepf 2002, Stephan and Gutknecht

Revision received November 7, 2008/Open for discussion until February 28, 2010.

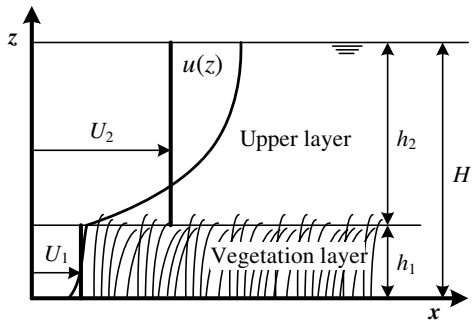

Figure 1 Schematic sketch of depth-limited open channel flows with submerged vegetation

2002, Wilson *et al.* 2003, Carollo *et al*. 2005) were used in laboratory experiments. It is known that the mean flow and turbulence flow structures with flexible stems do not differ significantly from those with rigid stems. However, the impact of stem flexibility on flow structures has rarely been explored.

The present study investigates the impact of stem flexibility on the mean flow and turbulence structures of depth-limited open channel flows with submerged vegetation. Laboratory experiments were carried out with simulated plant stems placed at the channel bottom. To observe the impact of stem flexibility, the drag force due to flexible stems was set similar to that due to rigid stems. Herein, these impacts on the flow structures are discussed, and general profiles of the mean flow and turbulence structures are presented.

2 Experiments

A tilting, straight, 8.0 m long and 0.45 m wide open channel facility at the Hydraulics Laboratory of Yonsei University was used for the laboratory experiments. Figure 2 shows a scheme of the open channel facility. The outlet and inlet structures were connected, allowing a continuous recirculation of discharge. As flow straighteners, 0.5 m long mats of punched aluminum panels were used to dampen the inlet turbulence and to eliminate swirl. Blocks with roughness elements were placed between the flow straightener and the vegetation panel to reduce the impact of emerging vegetation.

The instantaneous components of the streamwise u_i and vertical w_i velocities were measured using a Dantec® two-dimensional (2D) Laser Doppler Anemometer (LDA). The velocity components were measured along a vertical profile at the channel center 1.5 m upstream from the downstream end. Steady-uniform flow without wall effects was attempted before the tests were made. To clear the optical path of the LDA, two lines of model vegetation were removed. Using LDA, velocity data were sampled over 100 s, at 100–150 Hz. To remove the stem scale inhomogeneity within the vegetation layer, the sampled data were ensemble-averaged at three locations.

Table 1 lists the flow conditions employed in the experiments. Starting letters "F" and "R" in a test denote the use of flexible and rigid stems, respectively. For flexible stems, two discharges with three flow depths were generated. The channel slope was varied to render desirable flow conditions. Among six combinations, the case with the highest mean velocity was excluded because this was beyond the measuring range of the LDA. Since the degree of bending depends on the flow condition, the depth ratio H/h_1 was changed within 2.14 and 3.55. According to Raupach *et al*. (1996), who proposed that flows with depth ratios exceeding 5 to 10 are terrestrial canopy flows, the flows generated in the present study were depth-limited with submerged vegetation. In each test case, the bent heights of each individual stem were different, and changed with time. Thus, h_1 is the value averaged over the canopy and over time. To measure h_1 for flexible stems, ten different stems were selected, and the maximum and the minimum heights were measured for about 1 min. The Froude numbers $\mathsf{F} = U/(gH)^{0.5}$ and the Reynolds numbers ($\mathsf{R} = UH/\nu$) of the generated flows ranged between 0.15–0.41, and 15,700–26,300, respectively, indicating that the flows were subcritical and turbulent. Here, U is the depth-averaged mean velocity. For rigid stems, two test cases were conducted with different discharges under the one-flow depth condition.

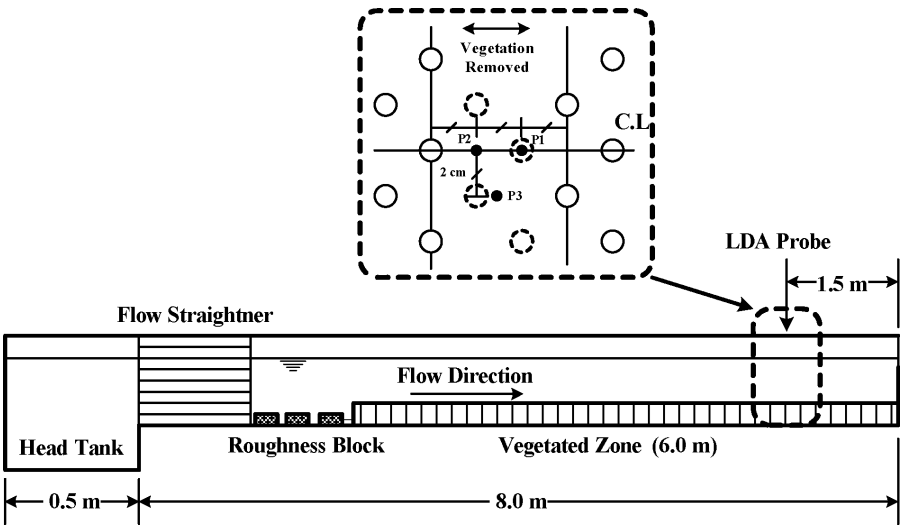

Figure 2 Scheme of open channel facility

Table 1 Experimental conditions

Case	Q [m^3/s]	H [m]	H/h_1 [-]	S [-]	u_* [m/s]	F_D [kg/ms^2]
FH1Q1	0.0075	0.055	2.44	0.00361	0.0339	2.053
FH2Q1	0.0075	0.075	2.73	0.00151	0.0265	1.519
FH2Q2	0.0105	0.075	3.00	0.00266	0.0361	2.648
FH3Q1	0.0075	0.110	3.24	0.00070	0.0229	0.646
FH3Q2	0.0105	0.110	3.55	0.00079	0.0247	0.843
RH2Q1	0.0075	0.075	2.14	0.00141	0.0235	1.475
RH2Q2	0.0105	0.075	2.14	0.00269	0.0325	2.721

Drags in two tests H2Q1 and H2Q2 were made similarly by setting flow conditions and channel slope approximately equal to balance the gravity effect by the stem drag for depth-limited open channel flows. Then, using measured velocity profiles, drag forces were estimated. The same values of drag coefficients, $C_D = 1.13$, were used for both flexible and rigid stems (Dunn 1996, Nepf and Vivoni 2000). The seventh column in Table 1 shows the estimated drags, indicating that the use of similar flow conditions and a channel slope results in similar values of drags.

Polyethylene films and cylindrical wooden dowels were used for flexible and rigid stems, respectively. For both stem types, the stem height was $h_p = 0.035$ m. The frontal-projected width and thickness of the polyethylene film were 0.002, and 0.0002 m, respectively, and the wooden dowel diameter was 0.002 m. The use of model vegetation with the same frontal-projected width ensured similar stem wake scales (Nepf *et al*. 1997, Poggi *et al*. 2004). The model vegetation was planted on a 1.2 m long, 0.45 m wide, and 0.01 m thick acryl plate. A total of five plates were mounted to create a 6.0 m long vegetation zone in the open channel facility. Herein, the stems were planted at the bottom in a staggered manner at regular spacing, i.e., 0.028 m apart in both the longitudinal and lateral directions. This resulted in a number of stems per unit area of $N = 1{,}400$ plants/m^2, corresponding to a vegetation density of $a = 2.78\,\mathrm{m}^{-1}$. Herein, for both flexible and rigid stems, the vegetation density a is defined with d as the diameter of cylindrical stems or the frontal-projected width of the film as

$$a = N \cdot d \tag{1}$$

The flexural rigidity of the polyethylene film used herein was evaluated according to Tsujimoto *et al.* (1996), based on the cantilever beam theory, resulting in $EI = 6.5 \times 10^{-6}\,\mathrm{Nm}^2$. An alternative method involved the formula of Kouwen and Li (1980)

$$EI = \gamma HS\left[3.4h_p\left(\frac{h_1}{h_p}\right)^{0.63}\right]^4 \tag{2}$$

where γ is the specific fluid weight and S is the channel slope. Equation (2) yields an estimate of $EI = 4.3 \times 10^{-6}\,\mathrm{Nm}^2$, slightly smaller than the value from the cantilever beam theory. As Kouwen and Li (1980) suggest that EI ranges for real grass from $5.0 \times 10^{-6}\,\mathrm{Nm}^2$ to $1.0 \times 10^{-3}\,\mathrm{Nm}^2$, the estimated value of the model vegetation has a flexural rigidity close to that of real grasses.

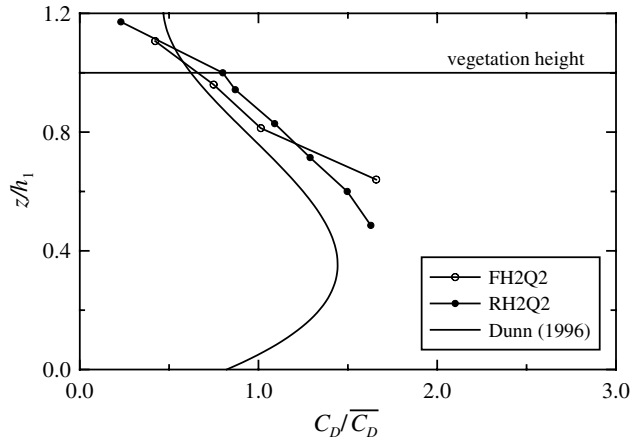

Figure 3 Vertical distribution of drag coefficient

3 Drag coefficient

For steady uniform flows with vegetation, the momentum equation in the streamwise direction may be written as

$$g^S - \frac{\partial \overline{uw}}{\partial z} - \frac{1}{2}aC_D u^2 = 0 \tag{3}$$

where g is gravitational acceleration, $-\overline{uw}$ Reynolds shear stress, C_D the drag coefficient, and u the streamwise mean velocity. The pressure is assumed to be hydrostatically distributed. Equation (3) states that the flow is made by balancing the gravity force with the resisting force due to Reynolds shear stress and drag. Figure 3 shows the vertical distribution of the drag coefficient. The drag coefficients for both the flexible and rigid stems are given, together with the empirical relationship by Dunn (1996)

$$\frac{C_D}{\overline{C_D}} = 0.74 + 3.51\left(\frac{z}{h_1}\right) - 6.41\left(\frac{z}{h_1}\right)^2 + 2.72\left(\frac{z}{h_1}\right)^3 \tag{4}$$

in which $\overline{C_D}$ is the depth-averaged value of C_D. This empirical relationship is the best-fit of Dunn's (1996) extensive laboratory measurements using both flexible and rigid stems. The vegetation density in Dunn's experiments ranged between $0.0069\,\mathrm{m}^{-1}$ and $0.0625\,\mathrm{m}^{-1}$. The above relationship describes the drag coefficient of parabolic shape with a maximum at about $z/h_1 = 0.33$. The results reveal that the estimated drag coefficient for flexible stems is nearly identical to that of rigid stems, and that both profiles agree well with the empirical relationship. The depth-averaged values of the drag coefficient $\overline{C_D}$ are 1.15 and 1.11 for flexible and rigid stems, respectively, i.e., close to $\overline{C_D} = 1.13$ from Eq. (4).

4 Mean flow and turbulence structures

Figure 4 shows the vertical distribution of the streamwise mean velocity. Two sets of test cases of similar drags are compared. The solid and dotted horizontal lines denote the stem heights prior and after bending, respectively. It can be seen that stem flexibility hardly affects the streamwise mean velocity. For the rigid stems, the inflection point of the mean velocity profile appears to be

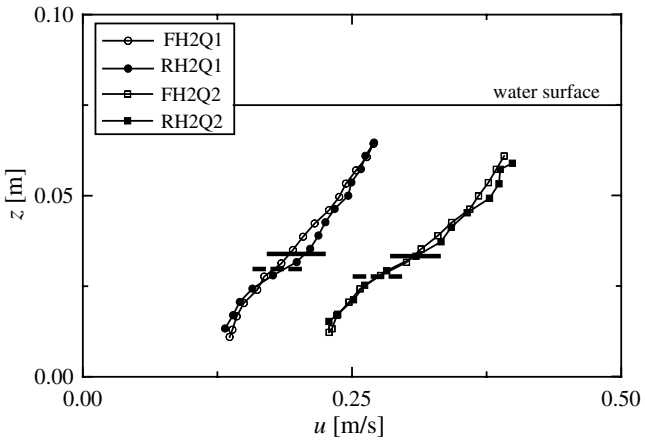

Figure 4 Impact of stem flexibility on mean velocity

located below the vegetation height. However, for the flexible stems, the inflection point cannot clearly be seen.

For depth-limited open channel flows with submerged vegetation, the mean velocity in the upper layer takes in general a log distribution (Ikeda and Kanazawa 1996, Lopez and Garcia 1998, Nepf and Vivoni 2000, Stephan and Gutknecht 2002), i.e.,

$$\frac{u(z)}{u_*} = \frac{1}{c_1}\mathrm{In}\left(\frac{z}{h_1}\right) + c_2 \tag{5}$$

in which u_* is the shear velocity at the interface between the upper and vegetation layers and c_1 and c_2 are constants. From laboratory tests with flexible stems, Kouwen *et al.* (1969) showed that c_1 is equal to the von Karman constant $\kappa = 0.41$.

Figure 5 shows the vertical distribution of the streamwise mean velocity. It can be seen that the mean velocity data collapse moderately in the upper layer $z/h_1 > 1$. The average values of c_1 are 0.39 and 0.42 for the flexible and rigid stems, respectively, which are close to κ. By contrast, the mean velocity data in the vegetation layer, looking quite uniform, do not collapse well. This seems to result from different depth ratios. According to Huthoff *et al.* (2007), the mean velocity in the vegetation layer is directly proportional to the square root of the depth ratio but inversely proportional to the square root of vegetation density and drag coefficient.

Yang (2009) reported that the slopes in Fig. 5 are different, depending on the vegetation density. That is, for flexible stems, Yang obtained $c_1 = 0.4$ and 0.11 for $a < 5.0\,\mathrm{m}^{-1}$ and for $a > 5.0\,\mathrm{m}^{-1}$, respectively, using regression analysis for literature data. The vegetation density of $a = 5.0\,\mathrm{m}^{-1}$ originates from Raupach (1994) and Poggi *et al.* (2004), who showed that u_*/u_{h1} is not affected by vegetation density if $a > 5.0\,\mathrm{m}^{-1}$. The respective ranges of c_2 are 5.1 to 6.2 and 2.2 to 3.0. This suggests that, for flexible stems, c_1 is close to κ if $a < 5.0\,\mathrm{m}^{-1}$, and $c_1 < \kappa$ if $a > 5.0\,\mathrm{m}^{-1}$. A reduction of von Karman constant was also suggested by Bayazit (1976), Nakagawa *et al.* (1991), and Dittrich and Koll (1997) for flows with small relative submergence. Nakagawa *et al.* (1991) attributed this to the dominance of the sweep events in the Reynolds stress near the bed. For depth-limited open channel flows with submerged vegetation, similar

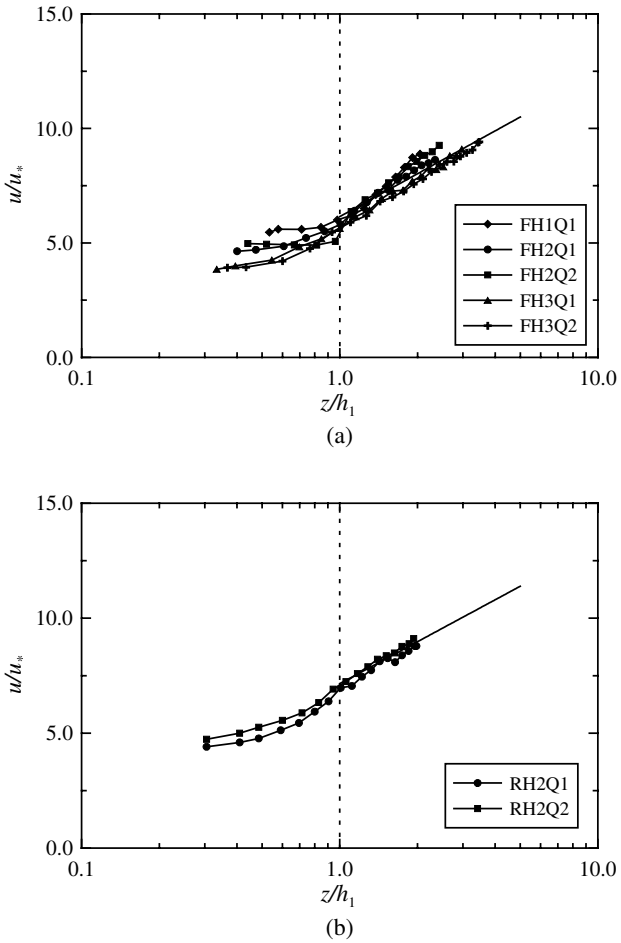

Figure 5 Vertical distribution of mean velocity for (a) flexible stems, (b) rigid stems

observations have also been reported by Nepf and Vivoni (1999) and are discussed below.

Similarly, for rigid stems, Yang (2009) obtained $c_1 = 0.39$ with $c_2 = 6.1$ to 7.2, and $c_1 = 0.13$ with $c_2 = 3.7$ to 4.2 for $a < 5.0\,\mathrm{m}^{-1}$ and $a > 5.0\,\mathrm{m}^{-1}$, respectively. These values are close to the constants for flexible stems, indicating that stem flexibility hardly affects the mean velocity. Therefore, it can be said that Eq. (5) holds for both flexible and rigid stems. However, the constants c_1 and c_2 depend on the vegetation density.

In Fig. 6, c_2 values from measured data are compared with Eq. (5). Note that c_2 fitted with Eq. (5) are in a good agreement with measured data. It is also noteworthy that the data can be divided into two groups, namely values for low vegetation density of less than $5.0\,\mathrm{m}^{-1}$ and those for high vegetation density greater than $5.0\,\mathrm{m}^{-1}$. Accordingly, the fitted c_2 values for low vegetation density lie within 5.2 to 7.1, and those for high vegetation density, between 2.0 and 4.1.

Figure 7 shows the vertical distribution of the Reynolds shear stress. The impact of stem flexibility can be seen by comparing test cases H2Q1 and H2Q2, for similar drags. In general, the Reynolds shear stress increases linearly from the water surface, with a maximum near h_1, and decreases toward the bottom. The impact of stem flexibility is the higher rate of change in the Reynolds shear stress. That is, the Reynolds shear stress increases

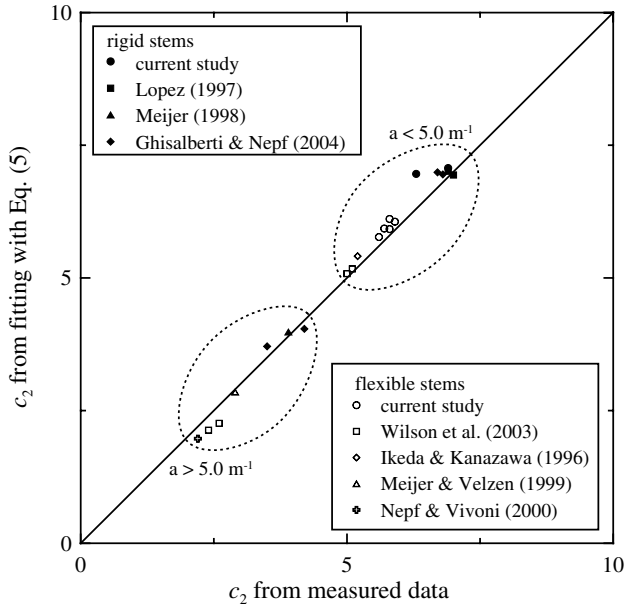

Figure 6 Comparison between measured and predicted c_2 values

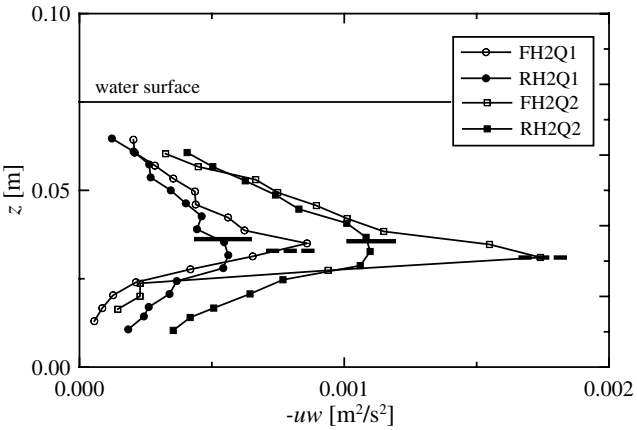

Figure 7 Impact of stem flexibility on Reynolds shear stress

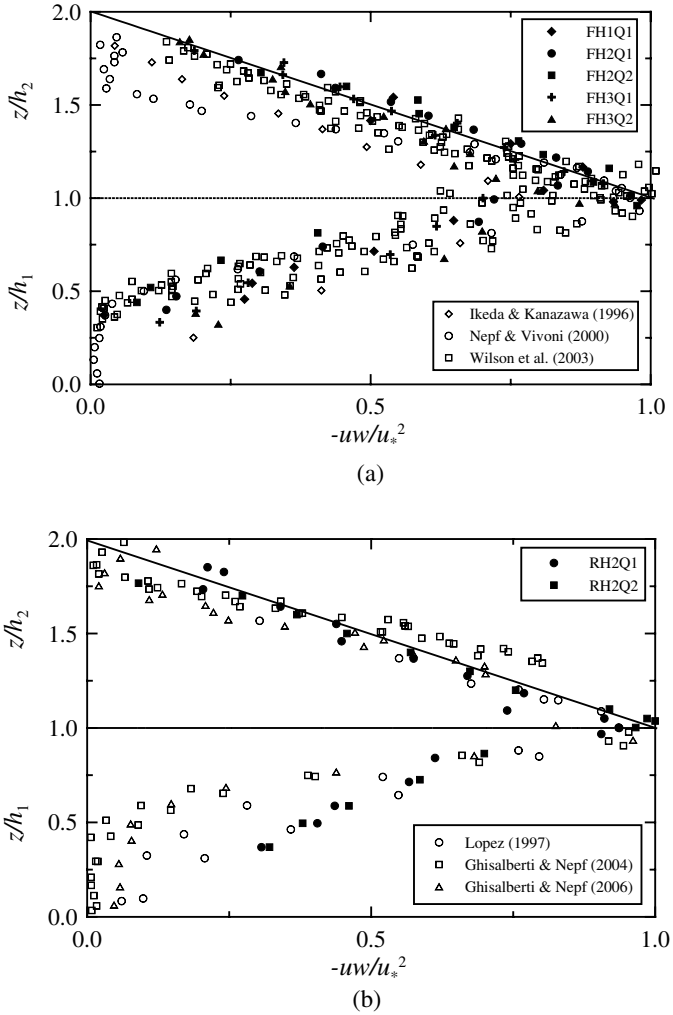

Figure 8 Vertical distribution of Reynolds shear stress for (a) flexible, (b) rigid stems

and decreases more rapidly to and from the maximum value for flexible stems, as compared with the profile of rigid stems. This results from enhanced temporal and spatial fluctuations of fluids near the interface caused by the swaying motions of flexible vegetation. A similar phenomenon was observed by Wilson *et al.* (2003).

Figure 8 shows the vertical distribution of the Reynolds shear stress for the flexible and rigid stems, respectively, together with the experimental literature data. The heights of the upper layer and the vegetation layer are used to normalize the vertical axis. In the upper layer, both profiles indicate that the Reynolds shear stress, zero at the free surface, increases linearly to the maximum near h_1. In the vegetation layer, the Reynolds shear stress for both the flexible and rigid stems decreases linearly to zero at about $z/h_1 = 0.3$ or 0.4. The height, at which the Reynolds shear stress becomes nearly zero, can be regarded as the penetration depth suggested by Nepf and Vivoni (2000). Below, the flow is similar to that with emergent vegetation. Moreover, in Fig. 8(a) for flexible stems, the peak of the Reynolds shear stress is sharp like in the profile for rigid stems.

The Reynolds shear stress profile can be used to estimate the shear velocity u_* at the interface. For test H2Q1, the shear velocity is estimated to 0.0265 m/s and 0.0235 m/s for the flexible and rigid stems, respectively. This indicates an approximately 13% increase in the interfacial shear stress due to stem flexibility under similar drags. Similarly, for test H2Q2, the shear velocities are 0.0361 m/s and 0.0325 m/s for flexible and rigid stems, respectively, indicating an 11% increase in the shear velocity due to the stem flexibility.

Figure 9 shows the estimated interfacial friction coefficient $C_{fi} = u_*^2/U_2^2$ against the Reynolds number. Measured data available in the literature are also plotted. The data, though scattered, indicate that the interfacial friction coefficient decreases with the Reynolds number. The best fit to the data is

$$C_{fi} = \exp(-1.61 \times 10^{-5} \cdot \mathsf{R}_2 - 4.08) \tag{6}$$

where $\mathsf{R}_2 = U_2 h_2/\nu$ is Reynolds number of the flow in the upper layer. Equation (6) can be used to assess the magnitude of the interfacial shear stress. That is, if one knows the average velocity over the whole depth, the mean velocity U_2 in the upper layer, which can be estimated according to Stone and Shen (2002) or by Huthoff *et al.* (2007), can be used to predict the interfacial shear stress.

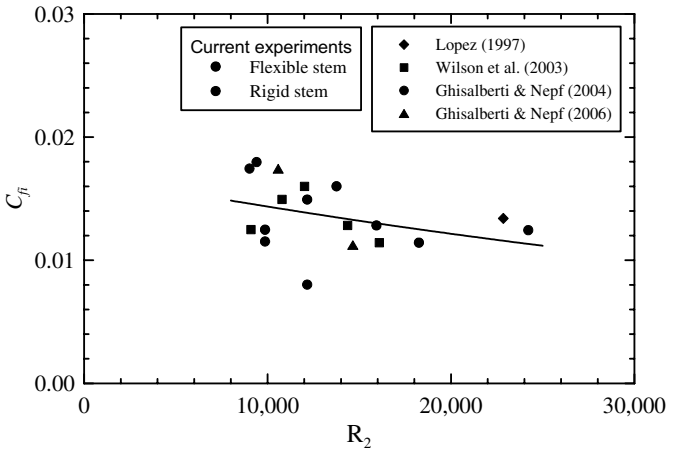

Figure 9 Interfacial friction coefficient versus Reynolds number R_2, (−−) Eq. (6)

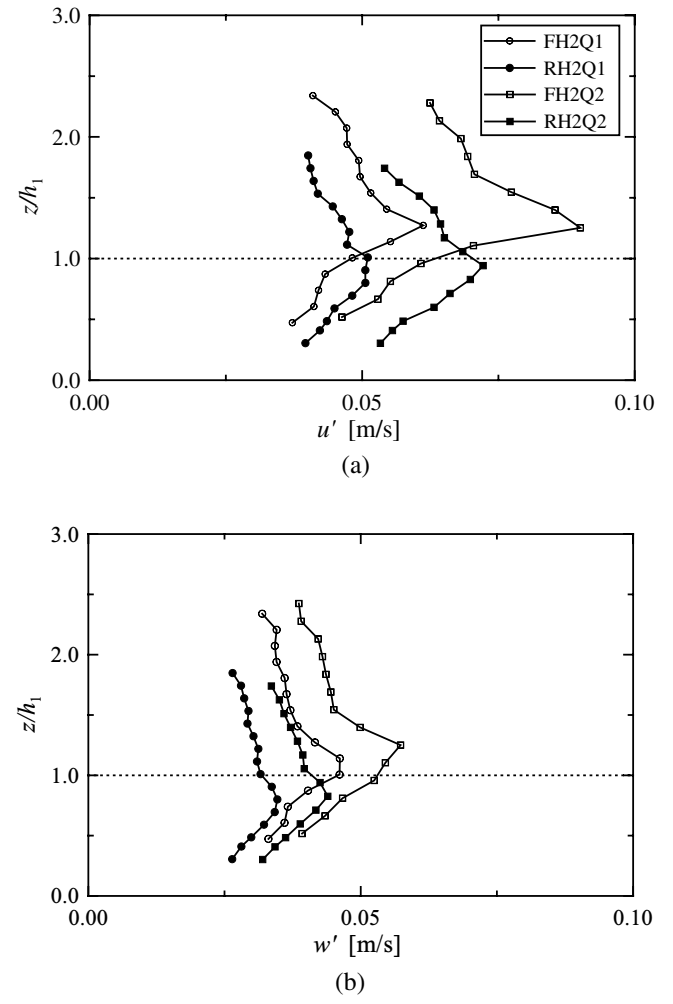

Figure 10 Impact of stem flexibility on turbulent intensity, turbulent intensity of (a) x-component, (b) z-component

Figure 10(a) shows the vertical distribution of the x-component turbulent intensity. The turbulent intensity is seen to increase from the water surface, having the maximum near the vegetation height, and then decreases toward the bottom. Note that the higher-inertia flow has a higher turbulent intensity. The impact of the stem flexibility can also be observed. That is, the turbulent intensity for the flexible stems is larger than that for the rigid stems in the upper layer. The location of the maximum turbulent intensity for the flexible stems appears to be slightly higher than the height of the vegetation layer. In contrast, for the rigid stem, the maximum is located at a height close to the vegetation layer. Note also that in the vegetation layer a reversal of the turbulent intensity occurs, i.e., the turbulent intensity for the rigid stems becomes larger than that for the flexible stems in the vegetation layer. Figure 10(b) shows the vertical distribution of the z-component turbulent intensity. The general shape of the profiles is similar to that of the x-component. The turbulent intensity for flexible stems can be seen to be larger than that for the rigid stems in both the upper and vegetation layers. This suggests that stem flexibility enhances the z-component turbulent intensity over the whole depth. Note also that the location of the maximum value of w' for rigid stems is lower than of flexible stems. This is similar to the distribution of u', resulting from the ignorance of the zero-plane displacement.

Figure 11 shows the normalized distribution of the turbulent intensity. Note that both components of the turbulent intensity collapse well. Both profiles reflect that the turbulent intensity has its maximum near the vegetation height and decreases toward both the free surface and the bottom. The plots for rigid vegetation are shown in Figs. 11(c) and 11(d). A similar trend and good collapse of the profiles is observed.

A regression analyses was conducted to develop expressions for turbulent intensity. For flows with flexible stems, the turbulent intensity is given by

$$\frac{u'}{u_*} = \exp\left[\frac{1}{1.13}\left(\frac{z}{h_1} - 0.5\right)\right] \quad \text{for } 0 \le z/h_1 \le 1 \tag{7a}$$

$$\frac{u'}{u_*} = \exp\left[\frac{1}{3.52}\left(2.5 - \frac{z}{h_1}\right)\right] \quad \text{for } 1 < z/h_1 \tag{7b}$$

$$\frac{w'}{u_*} = \exp\left[\frac{1}{1.22}\left(\frac{z}{h_1} - 0.8\right)\right] \quad \text{for } 0 \le z/h_1 \le 1 \tag{8a}$$

$$\frac{w'}{u_*} = \exp\left[\frac{1}{4.03}\left(1.7 - \frac{z}{h_1}\right)\right] \quad \text{for } 1 < z/h_1. \tag{8b}$$

For flows with rigid stems,

$$\frac{u'}{u_*} = \exp\left[\frac{1}{1.96}\left(\frac{z}{h_1} - 0.3\right)\right] \quad \text{for } 0 \le z/h_1 \le 1 \tag{9a}$$

$$\frac{u'}{u_*} = \exp\left[\frac{1}{3.71}\left(2.6 - \frac{z}{h_1}\right)\right] \quad \text{for } 1 < z/h_1 \tag{9b}$$

$$\frac{w'}{u_*} = \exp\left[\frac{1}{1.05}\left(\frac{z}{h_1} - 1.0\right)\right] \quad \text{for } 0 \le z/h_1 \le 1 \tag{10a}$$

$$\frac{w'}{u_*} = \exp\left[\frac{1}{2.75}\left(1.1 - \frac{z}{h_1}\right)\right] \quad \text{for } 1 < z/h_1. \tag{10b}$$

Figure 12 compares the profiles from these equations with the literature data. Note that the proposed relationships successfully predict the turbulent intensity. Comparing the turbulent

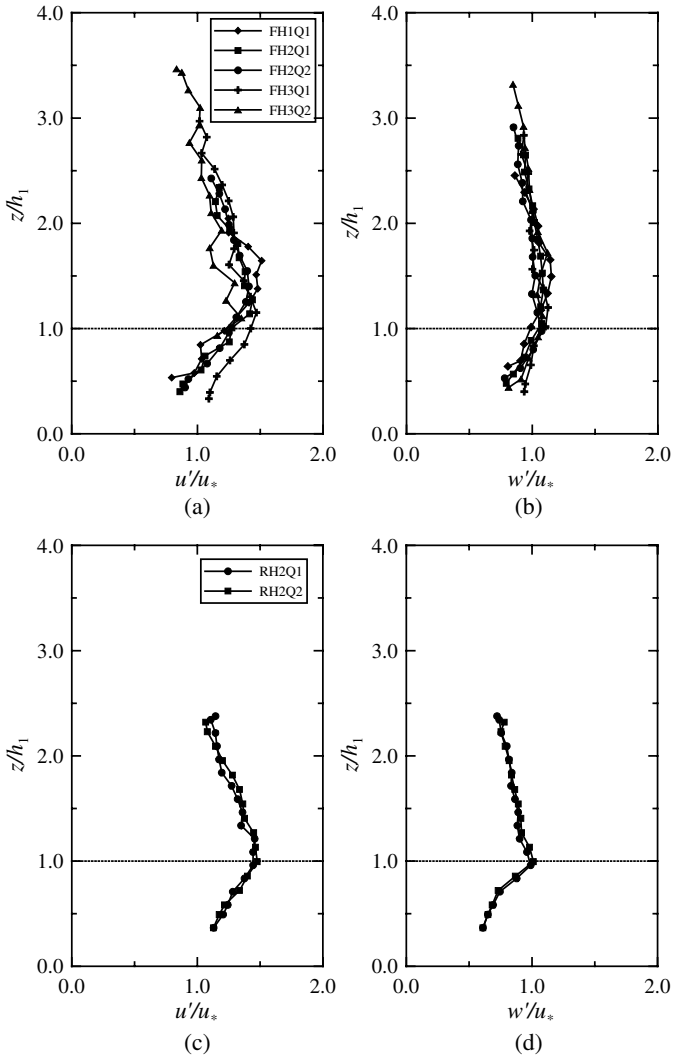

Figure 11 Vertical distribution of turbulent intensity, for (a) and (b) flexible stems, (c) and (d) rigid stems

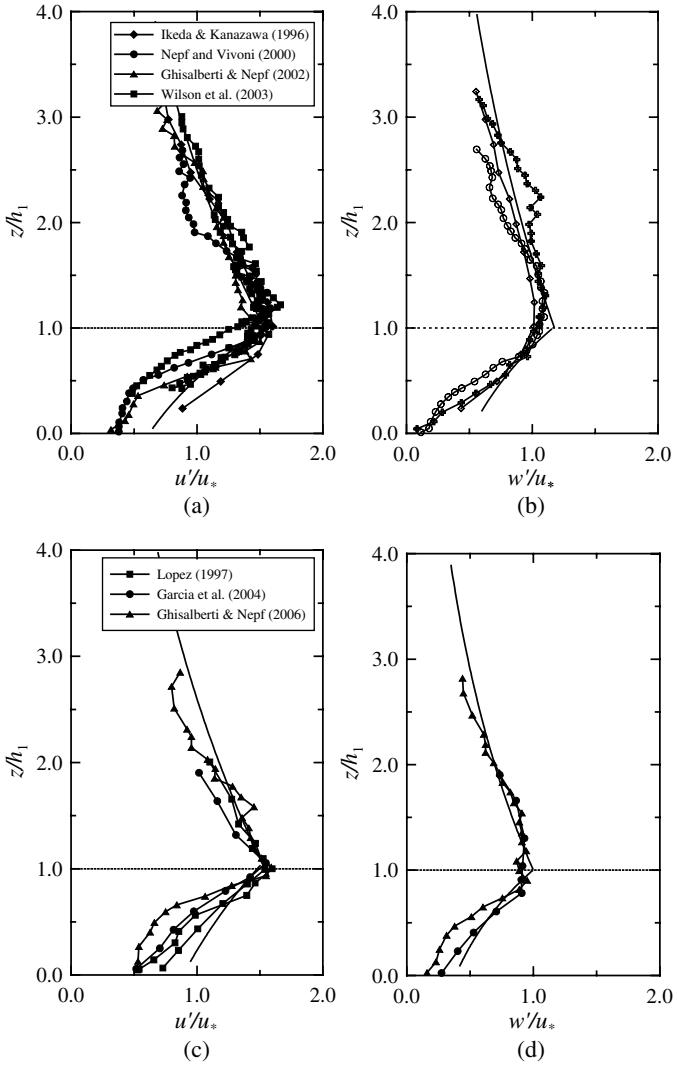

Figure 12 Prediction of turbulent intensity (data from literature), for (a) and (b) flexible stems, (c) and (d) rigid stems

intensity profiles in which the stem flexibility does not seriously affect u'/u_*, the turbulent intensity increases w'/u_* over the entire depth, leading to a profile similar to u'/u_*. This suggests that stem flexibility makes the turbulent flow more isotropic.

Figure 13 shows the power spectrum of the flow at three different heights. It can be seen that energy dissipation occurs within 10–20 Hz for both flexible and rigid stems, regardless the height. In addition, note that both spectrums show the energy-containing region by Kolmogorov's $-5/3$ theory. Table 2 lists the values of the turbulent kinetic energy (TKE) dissipation rate ε estimated by

$$E_{11}(f) = \alpha \varepsilon^{2/3} f^{-5/3} \tag{11}$$

where f denotes the 1D wavenumber, $E_{11}(f)$ is the 1D scalar energy density function of instantaneous streamwise velocity, and α the Kolmogorov constant, roughly equal to 0.55 in the outer layer and 0.51 in the inner layer of shear flows (Bradshaw 1967). The figure also shows is that, in the range of 0.1–1.0 Hz, the eddy generation in the flow with flexible stems is more vigorous than in the flow with rigid stems.

5 Quadrant analysis and turbulent kinetic energy budget

A quadrant analysis was performed and the contribution rates of each event to the Reynolds shear stress are given in Fig. 14. For both flexible and rigid stems, the contribution by sweeps (Q4) is larger in the vegetation layer. However, in the upper layer, ejections (Q2) make the major contribution to the Reynolds shear stress, regardless of stem flexibility. Inward and outward interactions take place uniformly over the entire depth, indicating that the Reynolds shear stress is generated mostly by sweeps and ejections in the vegetation and upper layers, respectively. Similar findings for flexible vegetation were presented by Nepf and Vivoni (1999) and Ghisalberti and Nepf (2004). The latter study confirms that stem flexibility does not seriously affect the generation mechanism of the Reynolds shear stress.

Figure 15 shows the turbulent kinetic energy budget for two test cases, FH2Q2 and RH2Q2. From Brunet *et al.* (1994), the TKE budget for flows with the canopy is

$$\frac{Dk}{Dt} = P_s + P_w + T_t + T_p - \varepsilon = 0 \tag{12}$$

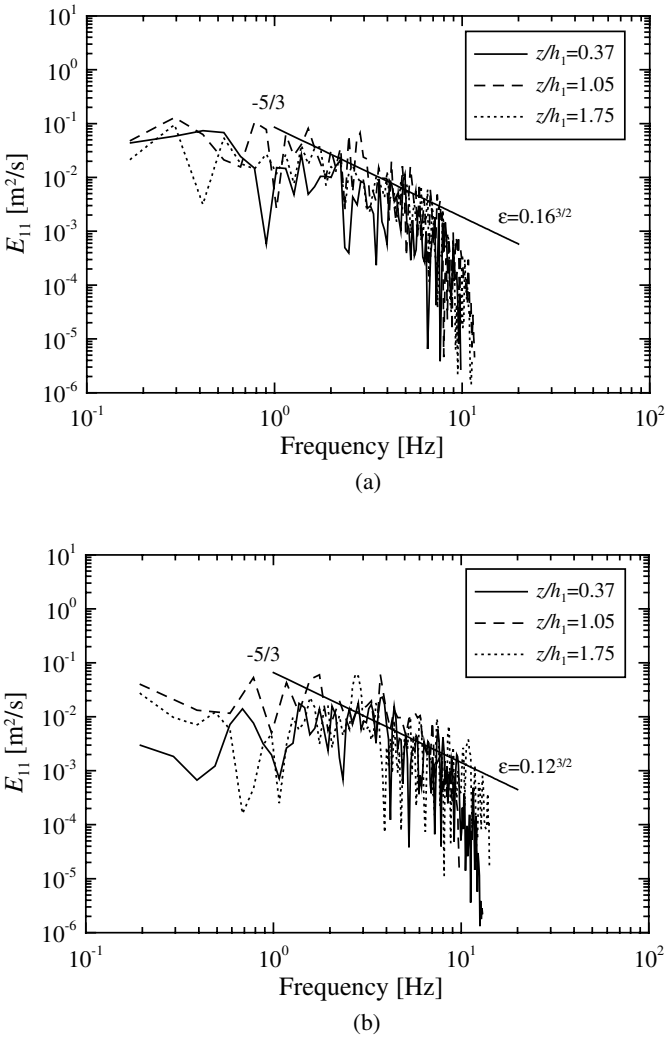

Figure 13 Power spectrum of FH2Q2 and RH2Q2 flows for (a) flexible stems (FH2Q2), (b) rigid stems (RH2Q2)

Table 2 Estimated turbulent kinetic energy dissipation rates

Case	ε_f [m²/s⁻³]	ε_r [m²/s⁻³]
H2Q1	0.056	0.035
H2Q2	0.064	0.042

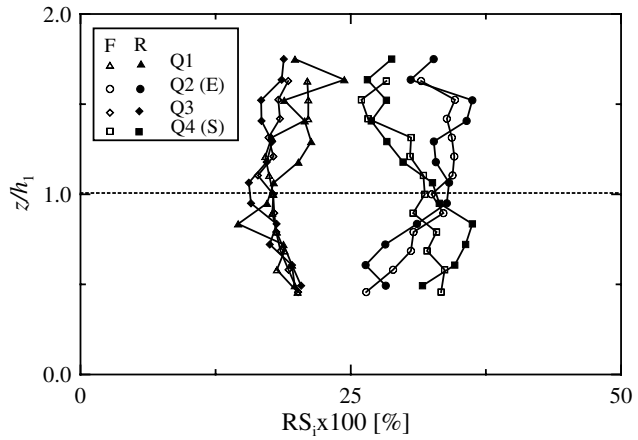

Figure 14 Vertical distributions of stress contribution rate

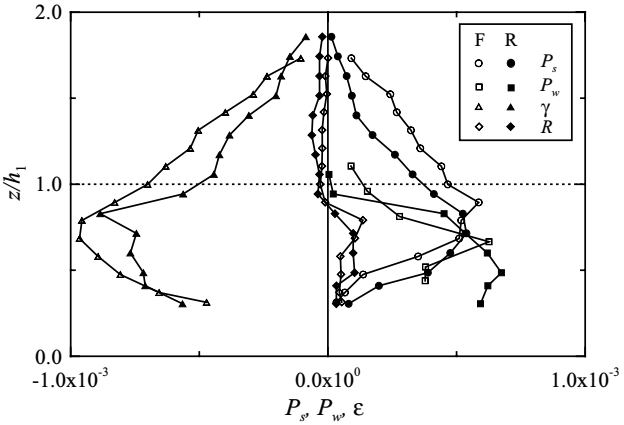

Figure 15 Turbulent kinetic energy budget for tests FH2Q2 and RH2Q2

where $P_s = -\overline{uw} \cdot \partial U/\partial z$ is the mean shear production, $P_w = 0.5 \cdot C_D \cdot a \cdot U^3$ the stem wake production, $T_t = \partial(w \cdot k)/\partial z$ the turbulence transport, and $T_p = \partial(w \cdot p)/\partial z$ the pressure transport. Since the turbulent kinetic energy k and instantaneous pressure p herein were neither evaluated nor measured, the terms T_t and T_p cannot be estimated. Fortunately, for depth-limited open channel flows with flexible submerged vegetation, Nepf and Vivoni (2000) indicated that the turbulence transport T_t has a similar magnitude, but is opposite in sign to the pressure transport T_p. This is confirmed herein by the small magnitudes of the residual R $(= T_t + T_p)$ over the entire depth.

In Figure 15, the vertical distributions of P_s, P_w, and ε are given. The TKE dissipation rate ε is estimated from the spectrum analysis. It is seen that both productions, by shear and wake, are nearly balanced by the TKE dissipation rate and that the overall distributions for the flexible stems are similar to those for the rigid stems. The wake production, increasing from the bottom, has a maximum at about $0.5h_1$ to $0.7h_1$ and decreases toward the vegetation height. It appears that the wake production by the rigid stems was slightly larger than that by the flexible stems. Similarly, the shear production has its peak slightly below h_1 and decreases toward both the bottom and the free surface. The shear production by the flexible stems is observed to be larger than that by the rigid stems, owing to the larger Reynolds stress, as seen in Fig. 7. The TKE dissipation rate profiles for both flexible and rigid stems have the peak at a location slightly lower than h_1, due to the wake production profile. Over the entire depth, ε for flexible stems appears to be larger as a result of the larger productions by the wake and the shear.

6 Conclusions

Laboratory experiments on open channel flows with submerged vegetation are presented. In the experiments, polyethylene films and wooden dowels were employed for flexible and rigid stems, respectively. An LDA was used to measure the 2D instantaneous velocities. To investigate the impact of stem flexibility, flows were compared with a similar drag characteristics but with different stems.

It was found that stem flexibility rarely affects the mean velocity. General profiles of the mean velocity are presented for both

the flexible and rigid stems. It was shown that the mean velocity takes a log-distribution in the upper layer and is relatively uniform in the vegetation layer. Specifically, in the log-profile for the upper layer, the constant c_1 related to the slope is close to the von Karman constant κ for both the flexible and rigid stems if the vegetation density is less than $5\ m^{-1}$. The ranges of the other constant c_2, as related to the intercept in the log-distribution, were also presented.

It became apparent that the stem flexibility increases the rate of change in the Reynolds shear stress, resulting in a larger maximum near the vegetation height. For both the flexible and rigid stems, the general profile of the Reynolds shear stress showed a linear increase and decrease toward the bottom in the upper and vegetation layers, respectively. The penetration depth, at which the Reynolds shear stress is nearly zero, was observed in the profile for the flexible stems, but not so for the rigid stems. Using the Reynolds shear stress profiles, the shear velocity at the interface between the upper and vegetation layers was estimated, resulting in an approximately 10% increase in the Reynolds shear stress, due to the stem flexibility. This is caused by enhanced swaying motions of flexible vegetation.

In addition, the stem flexibility was observed to increase both the streamwise and the vertical components of the turbulent intensity in the upper layer. In the vegetation layer, the stem flexibility increases the vertical component of the turbulent intensity; however, for the streamwise component, the turbulent intensity is reversed. Expressions for the turbulent intensity were proposed and compared with literature data, showing a good agreement. Upon comparing the general profiles of the turbulent intensity revealed that the stem flexibility enhances the level of the turbulence isotropy in flows with submerged vegetation.

A quadrant analysis was also carried out, revealing that the ejections (Q2) and the sweeps (Q4) are dominant in the upper layer and the vegetation layer, respectively. The impact of the stem flexibility on the generation of the Reynolds shear stress was not clearly observed. Finally, the turbulent kinetic energy budget was analyzed. It was found that the turbulent kinetic energy dissipation rate is balanced by the sum of the mean shear production and the stem wake production. The shear production due to flexible stems appeared to be dominant in the upper layer, leading to a larger turbulent kinetic energy dissipation rate for flexible stems over the entire depth.

These findings suggest that our previous knowledge on the mean flow characteristics for rigid stems remains unchanged even for flexible stems. However, a slight modification is needed in turbulence statistics, such as Reynolds shear stress and turbulence intensity. This is also true for the results from numerical modeling, whose governing equations are averaged over time and space with rigid cylindrical canopies.

Acknowledgments

This study was supported by the 2003 Innovation Project for Construction Technology (03-SANHAKYOUN-C01-01) through the Urban Flood Disaster Management Research Center in KICTTEP of MOCT KOREA. The Authors appreciate the comments offered by two anonymous reviewers.

Notation

a = Vegetation density ($= Nd$)
C_D = Drag coefficient
$\overline{C_D}$ = Depth-averaged drag coefficient
C_{fi} = Interfacial friction coefficient ($= u_*^2/U_2^2$)
c_1, c_2 = Constants in logarithmic velocity law;
d = Diameter of cylindrical stems or frontal-projected width of films
EI = Flexural rigidity of model vegetation
E_{11} = 1D scalar energy density function
F_D = Drag force due to vegetation ($= 0.5\rho a h_1 C_D U_1^2$)
F = Froude number ($= U/(gH)^{0.5}$)
f = 1D wave number
g = Gravitational acceleration
H = Total flow depth
h_1 = Height of vegetation layer
h_2 = Height of upper layer
h_p = Stem height
k = Turbulent kinetic energy
N = Number of stems per unit bed area
P_s = Mean shear production
P_w = Stem wake production
Q = Flow discharge
R = Reynolds number ($= UH/\nu$)
R_2 = Reynolds number of upper layer ($= U_2 h_2/\nu$)
S = Channel slope
T_t = Turbulence transport
T_p = Pressure transport
U = Mean velocity averaged over entire depth
U_1 = Mean velocity averaged over vegetation layer
U_2 = Mean velocity averaged over upper layer
u_{h1} = Mean velocity at the top of vegetation layer
u_i = Instantaneous component of streamwise velocity
u_* = Shear velocity ($= \max .[(uw)^{0.5}]$)
u' = Streamwise component turbulence intensity
w' = Vertical component turbulence intensity
w_i = Instantaneous component of vertical velocity
z = Distance measured from channel bed
α = Kolmogorov constant
ε = Turbulent kinetic energy dissipation rate
κ = von Karman constant ($= 0.41$)
ν = Kinematic viscosity

References

Bayazit, M. (1976). Free surface flow in a channel of large relative roughness. *J. Hydraul Res*. 14(2), 115–126.

Bradshaw, P. (1967). Conditions for the existence of an inertial subrange in turbulent flow. Report 1220. National Physics Laboratory of Aerodynamics, London UK.

Brunet, Y., Finnigan, J.J., Raupach, M.R. (1994). A wind tunnel study of air flow in waving wheat: single-point velocity statistics. *Boundary-Layer Meteorol.* 70, 95–132.

Carollo, F.G., Ferro, V., Termini, D. (2002). Flow velocity measurements in vegetated channels. *J. Hydraul. Engng.* 128(7), 664–673.

Carollo, F.G., Ferro, V., Termini, D. (2005). Flow resistance law in channels with flexible submerged vegetation. *J. Hydraul. Engng.* 131(7), 554–564.

Choi, S.U., Yang, W., Park, M.H. (2003). Turbulent and coherent structures of vegetated open channel flows affected by water depth. *KSCE J. Civil Engng.* 23(3B), 165–174 [in Korean].

Dittrich, A., Koll, K. (1997). Velocity field and resistance of flow over rough surfaces with large and small relative submergence. *Intl. J. Sediment Res.* 12(3), 21–33.

Duun, C.J. (1996). Experimental determination of drag coefficients in open channel with simulated vegetation. *MS Thesis*, University of Illinois, Urbana, IL.

Finnigan, J.J. (2000). Turbulence in plant canopies. *Annu. Rev. Fluid Mech.* 32, 519–571.

Garcia, M.H., Lopez, F., Dunn, C., Alonso, C. (2004). Flow, turbulence, and resistance in a flume with simulated vegetation. *Riparian Vegetation and Fluvial Geomorphology, Water Science and Application*, 8, 11–27, S.J. Bennet, A. Simon, eds.

Ghisalberti, M., Nepf, H.M. (2002). Mixing layer and coherent structures in vegetated aquatic flows. *J. Geophy. Res.* 107(C2), 3_1–3_11.

Ghisalberti, M., Nepf, H.M. (2004). The limited growth of vegetated shear layers. *Water Resour. Res.* 40, W07052.

Ghisalberti, M., Nepf, H.M. (2006). The structure of the shear layer in flows over rigid and flexible canopies. *Env. Fluid Mech.* 6, 277–301.

Huthoff, F., Augustijn, D.C.M., Hulscher, S.J.M.H. (2007). Analytical solution of the depth-averaged flow velocity in case of submerged rigid cylindrical vegetation. *Water Resour. Res.* 43(6), W06413.

Ikeda, S., Kanazawa, M. (1996). Three-dimensional organized vortices above flexible water plants. *J. Hydraul. Engng.* 122(11), 634–640.

James, C.S., Birkhead, A.L., Jordanova, A.A., O'Sullivan, J.J. (2004). Flow resistance of emergent vegetation. *J. Hydraul. Res.* 42(4), 390–398.

Kouwen, N. Li, R. (1980). Biomechanics of vegetative channel linings. *J. Hydraul. Div. ASCE* 106(HY6), 1085–1103.

Kouwen, N., Unny, T.E., Hill, H.M. (1969). Flow retardance in vegetated channel. *J. Irr. Drainage Div. ASCE* 95(IR2), 329–340.

Lopez, F. (1997). Open channel flow with roughness elements of different spanwise aspect ratios: Turbulent structure and numerical modeling. *PhD Thesis*, University of Illinois, Urbana IL.

Lopez, F., Garcia, M.H. (1998). Open channel flow through simulated vegetation: suspended sediment transport modeling. *Water Resour. Res.* 34(9), 2341–2352.

Meijer, D.G. (1998). Modelproeven overstroomde vegetatie. *Technical Report PR121*, HKV Consultants, Lelystad, NL [in Dutch].

Meijer, D.G., Velzen, E.H. (1999). Prototype-scale flume experiments on hydraulic roughness of submerged vegetation. Proc. 28th *IAHR Congress*, Graz, Austria, CD-ROM.

Nakagawa, H., Tsujimoto, T., Shimizu, Y. (1991). Turbulent flow with small relative submergence. *Lecture Notes in Earth Sciences*. Springer, Berlin.

Nepf, H.M., Sullivan, J.A., Zavistoski, R.A. (1997). A model for diffusion within emergent vegetation. *Limnology and Oceanography* 42(8), 1735–1745.

Nepf, H.M., Vivoni, E.R. (1999). Turbulence structures in depth-limited, vegetated flow: Transition between emergent and submerged regimes. Proc. 28th *IAHR Congress*, Graz, Austria, CD-ROM.

Nepf, H.M., Vivoni, E.R. (2000). Turbulence structures in depth-limited, vegetated flow. *J. Geophys. Res.* 105(C12), 28547–28557.

Nezu, I., Onitsuka, K. (2001). Turbulent structures in partly vegetated open channel flows with LDA and PIV measurements. *J. Hydraul. Res.* 39(6), 629–642.

Okabe, T., Hamai, N., Yuuki, T. (2000). Experimental study on hydrodynamic structure of flow on vegetated riverbeds. Proc. 12th *APD-IAHR Congress*, 311–319, Bangkok, Thailand.

Poggi, D., Porporato, A., Ridolfi, L. (2004). The effect of vegetation density on canopy sub-layer turbulence. *Boundary-Layer Meteorol.* 111, 565–587.

Raupach, M.R. (1994). Simplified expressions for vegetation roughness length and zero-plane displacement as functions of canopy height and area index. *Boundary-Layer Meteorol.* 71, 211–216.

Raupach, M.R., Finnigan, J.J., Brunet, Y. (1996). Coherent eddies and turbulence in vegetation canopies: The mixing-layer analogy. *Boundary-Layer Meteorol*. 78, 351–382.

Stephan, U., Gutknecht, D. (2002). Hydraulic resistance of submerged flexible vegetation. *J. Hydrol.* 269, 27–43.

Stone, B.M., Shen, H.T. (2002). Hydraulic resistance of flow in channels with cylindrical roughness. *J. Hydr. Engng.* 128(5), 500–506.

Tsujimoto, T., Shimizu, Y., Kitamura, T., Okada, T. (1992). Turbulent open channel flow over bed covered by rigid vegetation. *J. Hydrosci. Hydraul. Engng.* 10(2), 13–25.

Tsujimoto, T., Kitamura, T., Fujii, Y., Nakagawa, H. (1996). Hydraulic resistance of flow with flexible vegetation in open channel. *J. Hydrosci. Hydraul. Engng.* 14(1), 47–56.

Wilson, C.A.M.E., Stoesser, T., Bates, P.D., Pinzen, A.B. (2003). Open channel flow through different forms of submerged flexible vegetation. *J. Hydr. Engng.* 129(11), 847–853.

Yang, W. (2009). Experimental study of turbulent open-channel flows with submerged vegetation. *PhD Thesis*. Yonsei University, Korea.